Dyes and Pigments 194 (2021) 109617

Contents lists available at ScienceDirect

Dyes and Pigments

journal homepage: www.elsevier.com/locate/dyepig

Aggregation-induced emission-active hyperbranched polymers conjugated with tetraphenylethylene for nitroaromatic explosive detection

Nagendra Kalva, Chinh Hoang Tran, Min Woong Lee, Rimesh Augustine, Soo Jeong Lee, Il Kim *

School of Chemical Engineering, Pusan National University, Geumjeong-Gu, Busandaehak-Ro 63-2, Busan, 46241, Republic of Korea

ARTICLE INFO

Keywords:
Aggregation-induced emission
Hyperbranched polymers
Nitroaromatic compounds
Explosive detection

ABSTRACT

This work develops a facile synthesis for aggregation-induced emission (AIE)-active hyperbranched polyglycidols (HPGs) to design a solid-state sensor for detecting nitroaromatic explosives. The tetraphenylethylene moieties were conjugated onto the periphery of the HPGs in a single step using dynamic boronate ester cross-linkers. The resulting AIE-active HPGs exhibited excellent AIE characteristics in tetrahydrofuran (THF)/H_2O mixtures, emitting a strong blue fluorescence under UV irradiation. Dynamic light scattering and transmission electron microscopic analyses demonstrated that the self-assembled nanosized aggregates were stable in the THF/H_2O mixture. The fluorescence of the aggregates was dramatically quenched by various nitro compounds, including 2,4,6-trinitrophenol (or picric acid; PA), 2,6-dinitrophenol, 4-nitrophenol, 4-nitrotoluene, and nitromethane. The nano-aggregates exhibited extraordinary sensitivity towards PA, with a Stern–Volmer constant (K_{sv}) of 2.27 × 10^4 M^{-1} and a limit of detection of 40 ppb. Paper strips encapsulating the aggregates exhibited a vivid visual quenching, promising the practical applicability of these polymers as solid-state sensors for the detection of nitroaromatic explosives.

1. Introduction

In the past few decades, the sensitive and accurate detection of explosives and their precursors has become a pressing issue of global concern, owing to its implications for civilian and homeland security, and in combating the deepening terrorism crisis and the environmental pollution arising from the widespread use of such compounds in industries [1–7]. The most commonly used nitroaromatic explosives are 2,4,6-trinitrophenol (or picric acid; PA), 2,4,6-trinitrotoluene (TNT), and 2,4-dinitrotoluene (DNT). Exposure to trace amounts of these explosives has extremely detrimental effects on the skin, liver, eyes, kidneys, metabolism, and respiratory system in humans and animals [8–12]. Among these nitroaromatic explosives, PA has been widely used in lethal weapons and for the production of dyes, leather, ointments to treat burns, pharmaceuticals, fireworks, and rocket fuel [13]. In addition, the high acidity and water solubility of PA result in environmental pollution and eventually cause the contamination of soil and agricultural systems [14]. Therefore, it is essential to develop a highly sensitive sensor for the detection of nitroaromatic explosives. Various analytical techniques have been developed for the detection of nitroaromatic explosives, such as gas chromatography [15,16], X-ray imaging [17], Raman spectroscopy [18], mass spectroscopy [19], high-performance liquid chromatography [20], and ion-mobility spectrometry [21]. However, the use of these techniques is costly and time consuming, and requires large apparatuses and complicated operational procedures, limiting their practical field use.

Fluorescence-based probes have recently emerged as attractive candidates for explosive detection owing to their high sensitivity, cost-effectiveness, and lower time requirement for analysis [22–24]. Fluorescent co-polymers, nanofibers, quantum dots, metal-organic frameworks, and molecularly imprinted polymers have been developed for the detection of trace amounts of explosives using fluorescence-quenching methods [25–30]. All of these methods are based on the quenching of fluorescence by the transfer of electrons or energy between the electron-rich fluorescent molecules and the electron-deficient nitroaromatic compounds [31–35]. However, these fluorescence-based probes suffer from the self-quenching of their fluorescence at higher concentrations, which is called aggregation-caused quenching (ACQ) [36].

Recently, aggregation-induced emission (AIE), a phenomenon opposite to that of ACQ, was discovered by Tang and coworkers [37,38]. Although AIE materials are weakly-fluorescent in solution, they emit

* Corresponding author.
E-mail address: ilkim@pusan.ac.kr (I. Kim).

https://doi.org/10.1016/j.dyepig.2021.109617
Received 13 April 2021; Received in revised form 21 June 2021; Accepted 28 June 2021
Available online 29 June 2021

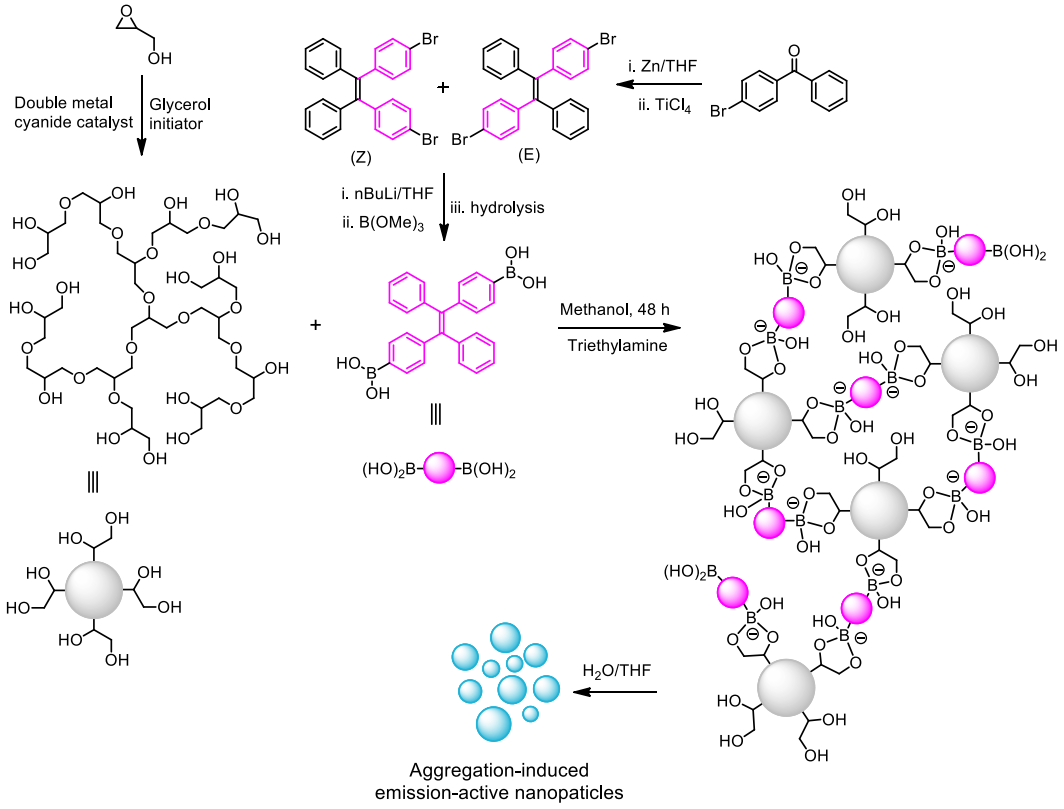

Scheme 1. Synthesis of the nano-sized AIE-active HPG-TPE aggregates that exhibit high sensitivity toward the detection of nitroaromatic explosives.

strong fluorescence in their aggregated state. A large variety of AIE-active molecules (AIEgens), such as tetraphenylethylene (TPE), triphenylamine (TPA), and distyrylanthracene derivatives, have been designed and explored for various applications including chemosensing, bioimaging, optoelectronics, and explosive detection [39–53].

Among these AIEgens, TPE derivatives have been widely employed for the construction of a variety of AIE materials, including small organic molecules, main-chain polymers, and hyperbranched polymers. For example, Ding et al. synthesized AIE-active moieties incorporated into the backbone and the side chain, and demonstrated their effectiveness at detecting nitroaromatic explosives [54]. Hyperbranched polymers conjugated with TPE moieties and their nanoaggregates have also been used for the detection of PA in aqueous solutions [55]. Tang and coworkers reported a series of TPE-conjugated polymers for the detection of explosive materials, particularly for PA in aqueous solutions [56]. For example, hyperbranched poly (aroxycarbonyltriazole) polymers incorporated with TPE units were synthesized using a metal-free click reaction and used for the detection of PA in tetrahydrofuran (THF)/water mixtures.

Hyperbranched polymers are a class of macromolecules having branched architectures with multifaceted functional groups on their peripheries [57]. Specifically, hyperbranched polyglycidol (HPG) polymers have attracted considerable interest because of their intrinsic hydrophilic, biodegradable, and multifunctional nature, and their easily accessible single-step syntheses compared to the tedious multistep syntheses of perfectly branched dendrimers [57–59]. Although great progress has been made on AIE-active hyperbranched polymers, the design of AIE-active materials based on commercially available HPG has rarely been reported [46,60].

In this study, a facile method was developed for the synthesis of TPE-based AIE-active HPG polymers. Multifunctional HPG with a molecular weight of approximately 1000 was initially synthesized using a newly developed protocol employing a commercially available heterogeneous double-metal cyanide (DMC) catalyst [61], following which the TPE moieties were cross-linked to the HPG periphery using boronic acid/diol interactions under weakly basic conditions to form boronated esters (Scheme 1). This single-step method is simple and eliminates tedious purification steps. The resulting cross-linked polymer shows no emission in organic solvents such as tetrahydrofuran and methanol. However, it exhibits a strong blue fluorescence upon the addition of water due to the AIE effect. The nanosized AIE-active HPG-TPE aggregates exhibited very high sensitivity toward the detection of nitroaromatic explosives.

2. Experimental

2.1. Materials

Glycidol (96%), *n*-butyllithium (2.5 M in hexane), titanium tetrachloride, and 2,4-dinitrophenol (DNP) were purchased from Sigma-Aldrich (Seoul, Korea) and used without further purification. 4-Bromobenzophenone, trimethyl borate, zinc dust, 4-nitrophenol (NP), 4-nitrotoluene (NT), nitromethane (NM), chloro-2,4-dinitrophenol and potassium carbonate were purchased from Acros Organics Company (New Jersey, USA). The HPG sample, having a molecular weight (MW) of approximately 1000, was synthesized according to a previously reported procedure [61] (refer to Supporting Information). PA was synthesized in a single step starting from phenol (caution: PA is an explosive and may explode from exposure to heat, flames, friction, or shock. Adding concentrated nitric acid to a solution of phenol in dimethyl sulfoxide is highly exothermic, and may cause the mixture to boil over. To prevent this, the nitric acid was added dropwise with careful cooling) [62]. Common solvents such as hexane, ethyl acetate, methylene chloride, and methanol were purchased from Duksan Chem. Co. (Daejeon, Korea), and distilled prior to use.

2.2. Instrumentation

^{1}H NMR (400 MHz) and ^{13}C NMR (100 MHz) spectra were recorded

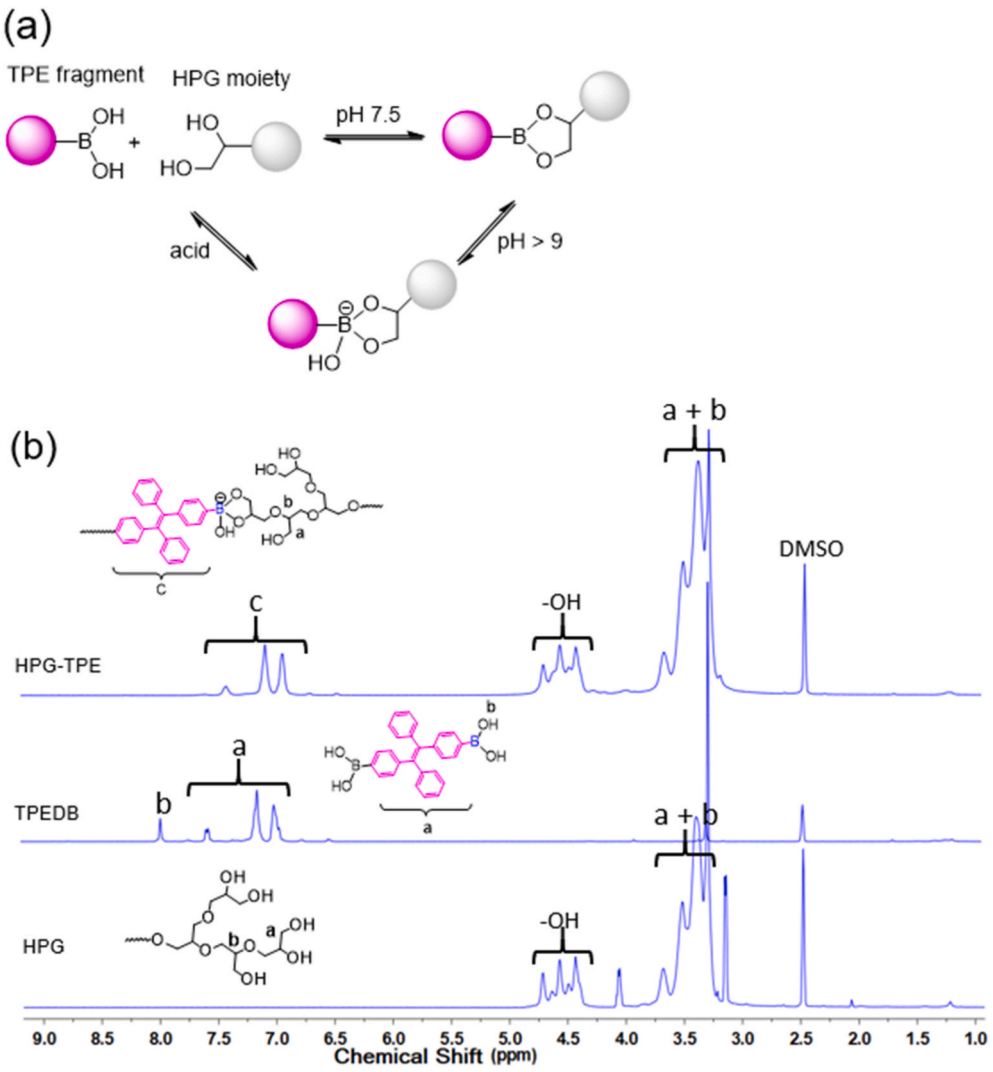

Fig. 1. (a) A plausible mechanism for dynamic diol exchange with boronic acid in response to pH, and (b) The ^{1}H NMR spectra of HPG, TPEDB, and the HPG-TPE conjugate in DMSO-d_6.

using a Varian INOVA 400 NMR spectrometer with tetramethylsilane as the internal standard. UV–visible spectra were recorded using a Shimadzu UV-1650PC, and a Shimadzu IR Prestige 21 spectrometer was used to record the Fourier-transform infrared (FT-IR) spectra using potassium bromide discs as the background in the range of 4000–600 cm^{-1}. Fluorescence emission spectra were recorded on a SCINCO Fluoro Mate FS-2 fluorescence spectrometer. The molecular weights (M_n) and polydispersity indices ($Đ$) of the polymers were recorded on a Waters gel permeation chromatography (GPC) system using dimethylformamide containing 0.1 N LiBr as the eluent at a flow rate of 1.0 mL min^{-1} and calibrated using monodisperse polystyrene. The dynamic light scattering (DLS) particle size distribution was obtained from a Nano ZS90 zeta potential analyzer (Malvern Instruments, Worcestershire, UK) using a He–Ne laser (633 nm), 90° collecting optics, and a Peltier temperature controller. The particle morphology was analyzed via transmission electron microscopy (TEM) using a JEOL-1299EX (JEOL, Peabody, MA, USA) operating at an accelerating voltage of 80 keV. The TEM samples were prepared in grids supported by a formvar film and treated with oxygen plasma (obtained from a Harrick plasma cleaner/sterilizer) for 15 s to render the surface hydrophilic. Time-resolved fluorescence measurements were carried out using a time-correlated single-photon counting (TCSPC) spectrometer [Quantaurus-Tau Fluorescence lifetime spectrometer C11367-31 Himamatsu photonics, Japan] with the detection wavelength at 480 nm for HPG-TPE both in the presence and absence of picric acid (Ex wavelength 340 nm).

2.3. Synthesis

1,2-Bis(4-bromophenyl)-1,2-diphenylethene (TPEDBr). Zinc dust (2.25 g, 34.7 mmol) and 4-bromobenzophenone (3 g, 11.5 mmol) were charged into a triple-neck round-bottom flask of 250 mL volume containing anhydrous THF (50 mL) at 0 °C. Subsequently, titanium tetrachloride (1.89 mL, 17.3 mmol) was added dropwise under argon flow. Following removal from the ice bath, the reaction mixture was stirred at room temperature for 30 min and thereafter refluxed for 12 h. Subsequently, the mixture was cooled to room temperature, quenched using a 10% aqueous solution of potassium carbonate, and extracted three times using methylene chloride. The purification of the crude product by column chromatography on silica gel using a mixture of hexane and ethyl acetate (3:1 v/v) as the eluent yielded a light-yellow solid (yield = 65%). ^{1}H NMR (400 MHz, $CDCl_3$): δ = 7.27–7.21 (m, 4H, Ar H), 7.14–7.10 (m, 6H, Ar H), 7.04–6.94 (m, 4H; Ar H), 6.86–6.90 (m, 4H; Ar H) ppm. ^{13}C NMR (101 MHz, $CDCl_3$): δ = 142.90, 142.81, 142.37, 142.27, 140.27, 132.96, 132.88, 132.86, 131.28, 131.20, 131.18, 131.09, 130.89, 130.83, 128.01, 127.86, 127.81, 127.76, 127.66, 126.93, 126.82, 120.78, 120.65.

4,4'-(2,2-diphenylethane-1,1-diyl)bis(1,4-phenylene) diboronic acid (TPEDB). Initially, 2 mL of *n*-Butyllithium (2.5 M in hexane) was

added dropwise to TPEDBr (0.8 g, 1.64 mmol) dissolved in THF (50 mL) at −78 °C. Following 1 h of stirring, 0.92 mL (8 mmol) of trimethyl borate was added, and the solution was allowed to react for 45 min. Thereafter, the solution was allowed to react overnight at room temperature. Following the completion of the reaction, 3 mL of 1 N HCl solution was added to quench the reaction. Following filtration and solvent removal, the purification of the crude product by column chromatography on silica gel using a mixture of ethyl acetate and methylene chloride (1:1 v/v) as the eluent yielded a yellow solid (yield = 56%). ^{1}H NMR (400 MHz, DMSO-d_6): δ = 7.93 (d, B(OH)$_2$), 7.54 (d, 4H; Ar H), 7.08–7.19 (m, 6H; Ar H), 6.93–6.97 (m, 8H; Ar H). ^{13}C NMR (101 MHz, DMSO-d_6): δ = 145.29, 143.59, 141.18, 141.08, 136.26, 134.03, 132.83, 131.10, 128.67, 128.23, 126.96.

HPG-TPE conjugates. TPEDB (0.126 g, 0.3 mmol, 3 equiv.) was dissolved in dry MeOH and triethylamine was added to adjust the pH to 9. Subsequently, HPG (0.1 g, ~1 mmol) dissolved in MeOH was added to the solution under stirring at 30 °C for 48 h. Following the completion of the reaction, the methanol was evaporated at a reduced pressure and precipitated in diethyl ether three times to obtain a sticky, viscous solid (yield = 95.3%). ^{1}H NMR (400 MHz, DMSO-d_6): δ = 7.44, (d, 4H, Ar H), 7.03–7.18 (m, 6H, Ar H), 6.87–7.02, (m, 8H, Ar H), 4.35–4.82 (−OH protons of HPG), 4.45, 3.15–3.80 (Br m, HPG backbone protons). ^{13}C NMR (101 MHz, CD$_3$OD): δ = 145.76, 143.06, 142.94, 133.65, 131.99, 131.17, 128.62, 127.26, 81.45, 79.93, 74.31, 72.66, 72.53, 71.07, 70.67, 64.69, 62.82, 58.90.

2.4. Fabrication of HPG-TPE nanoparticles

HPG-TPE nanoparticles were fabricated by dispersing the HPG-TPE conjugate in water at room temperature. Alternatively, water was added dropwise to the polymer solution dissolved in THF at room temperature. The volume fraction of water in THF (f_w) was varied in the range of 0–0.9 while maintaining a polymer concentration of 10 μg mL^{-1}.

2.5. Detection of nitro-explosives in aqueous solution

The detection of nitro explosives was performed using the fluorescence-quenching behavior of the HPG-TPE nanoparticles in an aqueous THF (f_w = 0.9). Nitro-explosive analytes dissolved in a mixture of THF and water (f_w = 0.9) were individually added to quartz cuvettes containing 3 mL each of the aforementioned nanoparticle-containing solution, and the emission intensity was recorded following excitation at 330 nm through emission slits of 5 nm width.

The detection limit of nitro explosives was determined using PA based on previously reported procedures [63,64]. The fluorescence titration of HPG-TPE nanoparticles in THF/H$_2$O (f_w = 0.9) mixture using PA was performed by adding aliquots of PA solution. The fluorescence intensity was plotted as a function of the amount of PA added. A sharp change in the fluorescence intensity was observed in this plot, corresponding to the PA concentration (C_T). The detection limit was obtained by multiplying C_T with the concentration of the polymer (10 μg mL^{-1}).

The visual detection of PA was performed under UV light on strips of paper coated using the nanoparticle-containing solution. A piece of filter paper was immersed in a THF/H$_2$O (f_w = 0.9) solution containing HPG-TPE nanoparticles (10 μg mL^{-1}) for 10 min. Thereafter, the filter paper was dried in vacuum at 50 °C for 24 h. When irradiated by a UV lamp at 365 nm, this filter paper fluoresced strongly, whereupon it was photographed.

3. Results and discussion

3.1. Synthesis and characterization of HPG-TPE conjugates

The AIE-active HPG-TPE conjugate was synthesized as shown in Scheme 1. Boron-polyol interactions are of fundamental importance to human health, plant growth, and quorum sensing in certain bacteria. Complexes between boron and sugars, which are reversible in aqueous solutions, have become critical to the development of synthetic carbohydrate receptors. The covalent product between a boronic acid and a diol is termed a boronate ester, since it is analogous to a carboxylate ester. The AIE-active HPG-TPE conjugate was synthesized through the formation of a well-known dynamic covalent bond between the hydrophobic phenyl boronic acid-mediated AIE dye (TPEDB) and the diol groups of HPG (Fig. 1(a)). TPEDB was initially synthesized according to a previously reported procedure [65], and its structure was confirmed using ^{1}H NMR and ^{13}C NMR spectra (Fig. 1 and Figs. S3–S5 in the Supporting Information). The peaks at 7.54–6.97 ppm are assigned to aromatic protons, suggesting the successful synthesis of TPEDB. A hyperbranched polymer (HPG) was synthesized using a procedure previously reported by our group.[61] The quantitative analysis of the resulting HPG using its ^{13}C NMR spectrum (Fig. S1) estimated its molecular weight (MW), degree of branching (DB), and number-average degree of polymerization (DP_n) as 962, 0.51, and 13, respectively. The average number of terminal diol groups in the polymer was 6. The dynamic phenyl borate bonds are formed by the facile reaction between TPEDB and the diol groups of HPG at room temperature by adjusting the pH of the solution to 9 using triethylamine.

Highly refined syntheses and tedious workup procedures have been required for the preparation of TPE-conjugated hyperbranched poly-

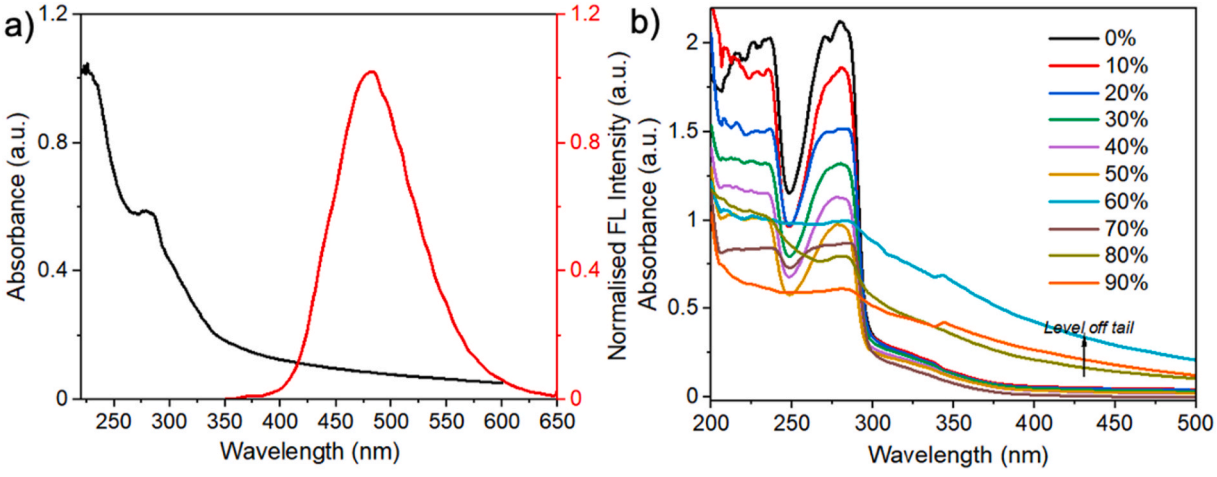

Fig. 2. a) The UV–Vis and fluorescence spectra of HPG-TPE nanoparticles formed at f_w = 0.9. B) The absorbance spectra of the HPG-TPE nanoparticles formed in various volume fractions of water (f_w = 0 to 0.9) in THF.

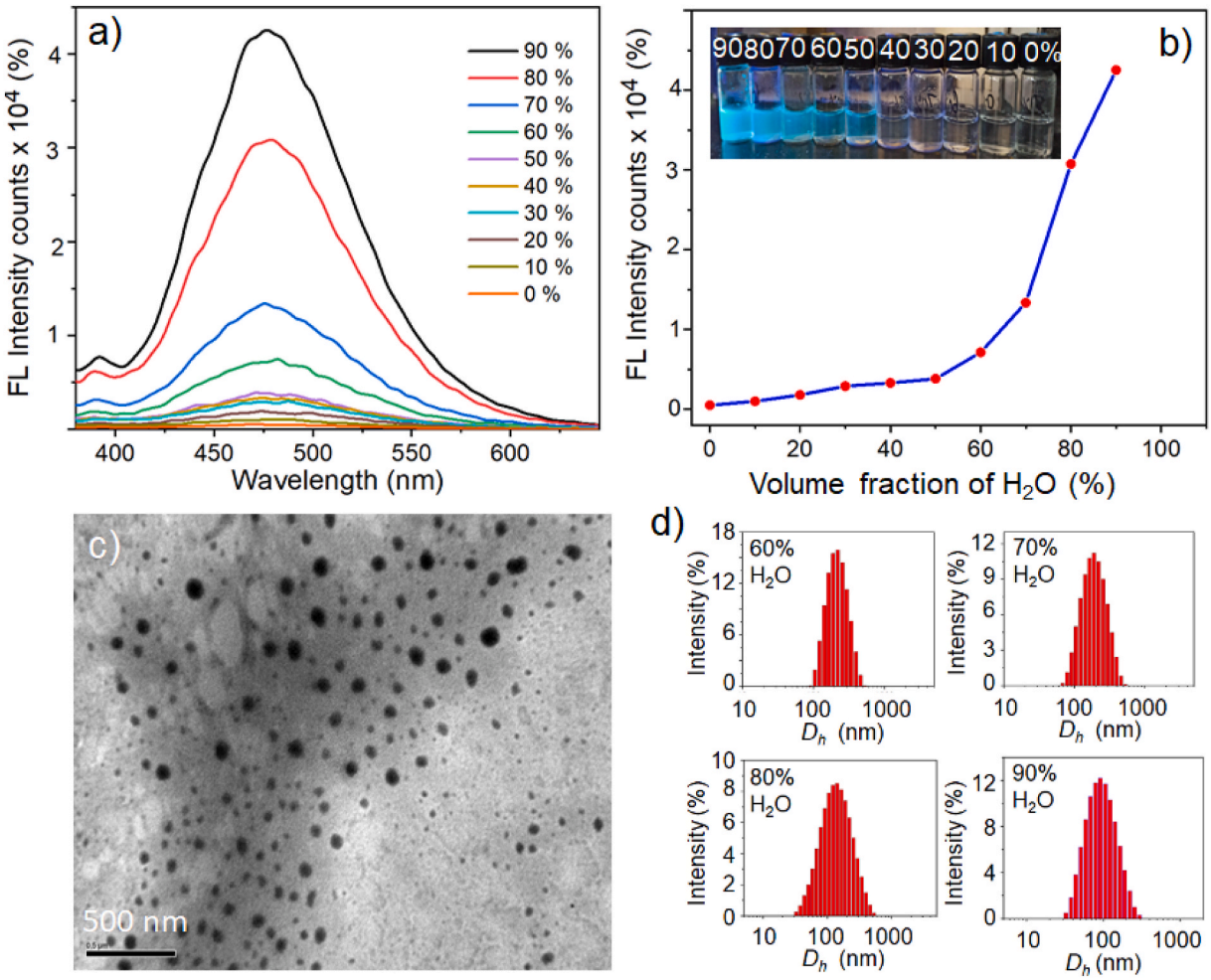

Fig. 3. a) The fluorescence spectra of the HPG-TPE conjugates formed in various volume fractions of water (f_w = 0 to 0.9) in THF, obtained at the excitation wavelength of 330 nm and the HPG-TPE concentration of 10 μM, b) the relationship between fluorescence intensity and fraction of water, c) TEM image of nanoparticles at f_w = 0.9, and d) DLS histograms of AIE-active nanoparticles formed at various fractions of water between f_w = 0.6 and 0.9.

mers to date. For example, hyperbranched poly (aroxycarbonyltriazole)s were prepared by the metal-free click polymerization of tripropiolates and TPE-containing diazides [56]. A carboxyl-functionalized hyperbranched polymer, poly (3-ethyl-3-oxetanemethanol)-*star*-poly (ethylene oxide) (HSP) was subjected to an addition reaction with TPE containing 2-((4-(1,2,2 triphenylvinyl)phenethyl)thio)ethanol to afford hyperbranched HSP-TPE copolymers [55]. Compared to the existing methods for preparing AIE-active hyperbranched polymers, the single-step synthesis described here is easily accessible. The methanolic HPG solution was directly added to the solution of TPEDB in methanol at 30 °*C* and pH 9, and stirred for 48 h. The resulting reaction mixture was precipitated in diethyl ether to produce pure AIE-active HPG-TPE as a sticky solid. The chemical structure was confirmed using ^{1}H and ^{13}C NMR spectroscopy (Fig. 1 and Fig. S6 in Supporting Information). The peaks appearing at 6.96–7.44 ppm were attributed to signals from aromatic protons adjacent to the boronate ester groups due to the upfield shift of H on the β-carbon, confirming the formation of boronate ester bonds and HPG-TPE. The resultant polymer HPG-TPE was analyzed by using DMF GPC, showing a monomodal peak that shifts towards a higher molecular weight than HPG. The Mn and *Đ* values estimated from GPC for polymers HPG and HPG-TPE were 2.5 KDa, 11.8 KDa and 1.35, 1.88 respectively (Fig. S2). In addition, FT-IR spectra were also used to confirm the structure of the final polymer HPG-TPE. The new stretching vibration at 1347 cm^{-1} for boronate ester bond (–B–O–) confirmed the successful synthesis of HPG-TPE polymer (**Fig. S7**).

3.2. Photophysical properties of HPG-TPE nanoparticles

The photophysical properties of the HPG-TPE nanoparticles were characterized by UV–Vis and fluorescence spectroscopy. The amphiphilic HPG-TPE polymer self-assembles into core-shell nanoparticles by forming a hydrophobic TPE core and a hydrophilic hydroxyl groups of HPG extended on the periphery. The polymer HPG-TPE sample was dissolved in THF and varying amounts (f_w = 0.1–0.9) of water were added to the solution while maintaining a constant polymer concentration. The scattering intensity varied significantly with the concentration of water. As the amount of water increases, the hydrophobic TPE moieties may form nuclei due to their assembly and aggregation, causing the particles to grow. The resulting solution, containing the aggregated nanoparticles, became AIE-active materials. As shown in Fig. 2a, the HPG-TPE nanoparticles formed at f_w = 0.9 were excited in the wavelength range of 230–380 nm, whereupon the absorption maximum was located at 286 nm. As expected, the nanoparticles emitted a strong blue fluorescence in the range of 380–600 nm with the emission maximum being located at 480 nm when excited at different wavelengths (230–380 nm). In Fig. 2b, the UV–Vis spectra of HPG-TPE polymer in different THF and water fractions are displayed. The absorption spectrum of polymer HPG-TPE shows an absorbance band at 278 nm. Upon increasing the water fraction from 0 to 50%, the absorption peak at 278 nm is monotonously decreased. Then, increasing water fraction from 60% to 90% the broadening of absorption peak is observed with bathochromic shift 8 nm from 278 to 286 nm.

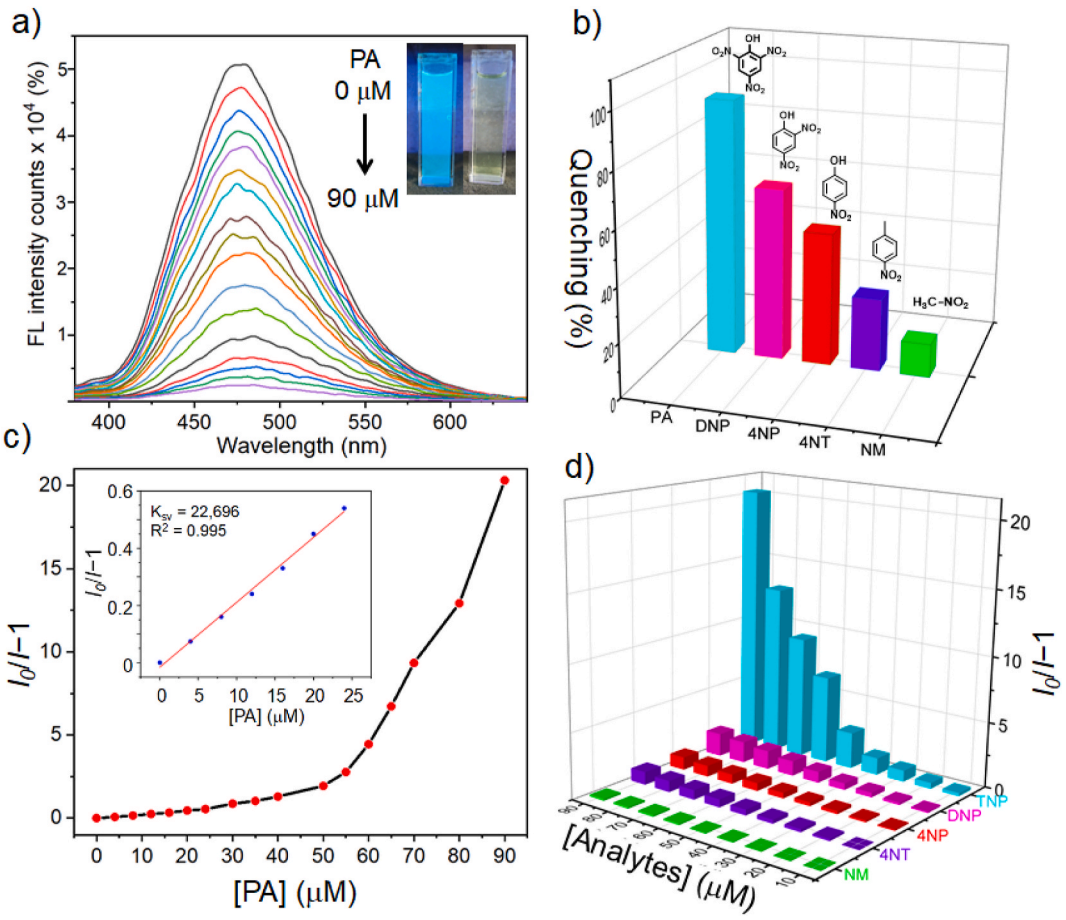

Fig. 4. a) The fluorescence spectra of the HPG-TPE nanoparticles (10 μM) in $f_w = 0.9$ recorded during the stepwise addition of PA to HPG -TPE nanoparticles up to a concentration of PA of 90 μM, at which concentration the fluorescence was completely quenched (inset image), b) the percentage of fluorescence quenched by the addition of different nitro-explosives, c) the Stern–Volmer plot ($(I_o/I-1)$ versus PA concentration) of relative fluorescence intensity, and d) a plot of fluorescence intensity versus the concentration of various nitro-analytes in an aqueous mixture.

Additionally, the 'levelling off tail' was observed in the UV–Vis spectra, suggesting the formation of aggregates of HPG-TPE.

The AIE effect of HPG-TPE nanoparticles was investigated by measuring their fluorescence in solvent-mixtures of water and THF. Upon increasing the volume fraction of water from $f_w = 0$ to 0.1, to 0.3, and finally to 0.50, the overall increased solvent polarity twisted the HPG-TPE molecules, causing insufficient aggregation of the TPE moieties by π–π stacking. However, the fluorescence intensity increased remarkably upon increasing $f_w = 0.7$ to 0.9 (Fig. 3a and **b**). Under these conditions, HPG-TPE preferably forms nanoclusters, leading to restricted intramolecular motion, resulting in the AIE effect. The fluorescence quantum yield (Φ_F) measured for HPG-TPE nanoparticles formed at $f_w = 0.9$ was 62.1%, which was much higher than that obtained in pure THF (0.29%). DLS measurements showed that the size of the nanoparticles (Fig. 3c and d) decreased as the fraction of water increased. The average hydrodynamic diameter of the nanoparticles was 220.5, 191.7, 141.8, and 103.2 nm in solutions of at $f_w = 0.6$, 0.7, 0.8, and 0.90, respectively. In addition to the variation in polarity caused by the increase in the fraction of water, the increase in the viscosity of the medium may correlate to the aggregation behavior or the AIE effect because the restriction of torsional and vibrational motions of the polymer may induce a change in viscosity. The viscosities of pure THF and pure water were 0.463 and 0.754 mPa s at 303.15 K, respectively [66]. The viscosity increased up to 1.384 mPa s at $f_w = 0.6$, and thereafter decreased monotonically to 1.341 and 1.003 mPa s at $f_w = 0.7$ and 0.9, respectively. Considering that the sizes of the nanoparticles as measured by DLS were 220.5, 191.7, 141.8, and 103.2 nm at $f_w = 0.6$, 0.7, 0.8, and 0.90, respectively (Fig. 3d), the viscosity and polarity of the solvent influence the nucleation, aggregation, coalescence, and growth of the particles following the Ostwald ripening mechanism. The nanoparticles formed at $f_w = 0.9$ were spherical in shape with an average size of 92 ± 3.2 nm (Fig. 3c). The average size of the micelles measured using TEM was slightly smaller than that measured using DLS (103.2 nm), owing to the drying of the solvents during sample preparation.

3.3. Detection of nitroaromatic compounds in aqueous solution

Highly sensitive and selective detection of ultra-trace analytes from nitroaromatic explosives such as PA, TNT, and DNT has attracted attention because explosives are important chemical species for detection in mine fields, military applications, munitions remediation sites, and homeland security applications. Phenolic nitro compounds, such as TNP and DNP, are highly soluble in water and can contribute majorly toward environmental pollution and health hazards caused by soil and groundwater contamination. TPE derivatives possess the ability to detect nitro explosives because of their highly localized π-electron transfer from TPE derivatives to the low LUMO energies of nitroaromatics [47–49]. Taking advantage of this, HPG-TPE nanoparticles fabricated in at $f_w = 0.9$ at a concentration of 10 μM were used for the detection of nitroaromatic compounds using PA, DNP, NP, NT, and the aliphatic nitro explosive, nitromethane, (NM), as model explosives. As shown in Fig. 4a, as the stock solution of PA was added to the TPE-HPG nanoparticles, the fluorescence was gradually quenched at 480 nm. The fluorescence was eventually completely quenched, and the quenching

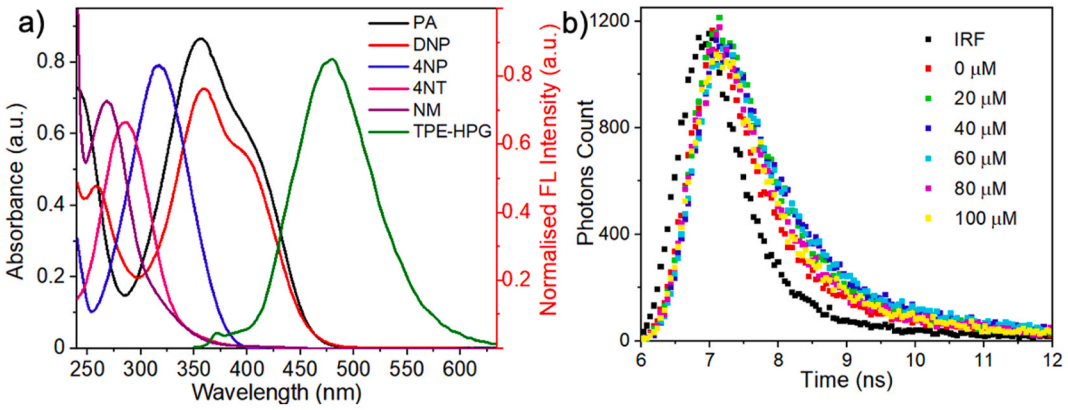

Fig. 5. a) Absorbance spectra of various explosive analytes and emission spectra of HPG-TPE nanoparticles in THF/H_2O (1:9 v/v) mixture; b) time-resolved fluorescence spectrum of HPG-TPE nanoparticles (10 μM) in THF/H_2O (1:9 v/v) mixture with addition of the increasing concentrations of PA from 0 μM to 100 μM λ_{em} = 480 nm. All the emission spectra were taken with λ_{ex} = 340 nm.

efficiency for PA was approximately 95% at a PA concentration of 90 μM. At the same analyte concentration, the quenching efficiencies of DNP, NP, NT, and NM were 64%, 49%, 27%, and 12%, respectively (Fig. 4b). These results indicate that significant fluorescence quenching occurs specifically with phenolic nitroaromatics.

To understand the process of quenching of HPG-TPE nanoparticles due to the addition of nitroaromatic explosives, the Stern–Volmer relationship was employed:

$$\frac{I_0}{I} = K_{sv}\,[Q] + 1 \quad (1)$$

where I_0 is the initial fluorescence intensity in the absence of the analyte, I is the fluorescence intensity in the presence of the analyte, [Q] is the molar concentration of the analyte, and K_{sv} is the quenching constant in M^{-1}. The inset of Fig. 4c displays a Stern–Volmer plot of the relative fluorescence intensity ($I_0/I-1$) versus [PA]. K_{sv} was calculated as 2.27×10^4 M^{-1} by fitting a linear plot to the Stern–Volmer equation at a low concentration of PA (25 μM). The limit of detection of PA by the HPG-TPE nanoparticles was found to be 40 ppb (Fig. S8 in the Supporting Information). The quenching curve deviated from linearity and bent upward at a [PA] higher than 25 μM, suggesting an amplified quenching effect [48]. The K_{sv} values were 8.25×10^3, 6.69×10^3, 2.9×10^3, and 2.3×10^3 M^{-1} for DNP, NP, NT, and NM, respectively (Fig. 4d). Therefore, the fluorescence quenching efficiency decreased in the order PA ≫ DNP > NP > NT > NM.

3.4. Sensing mechanism of nitroaromatics

The nonlinear Stern-Volmer plot curvature for PA suggested the combination of static quenching and dynamic quenching. The resonance energy transfer can occur from the sensor to the analyte if the sensor and analyte are close to each other and the absorption band of the analyte has an effective overlap with emission band of the sensor. In order to test the possibility of resonance energy transfer from the sensor (donor) to the analyte (acceptor), we plotted the absorption spectra of nitroaromatics along with the fluorescence spectrum of the sensor. Fig. 5a shows that the absorption spectra of PA and DNP has a large overlap with the emission spectrum of HPG-TPE nanoparticles, whereas a negligible overlap is observed for other nitroaromatics 4NP, 4NT and NM. This result suggests, the quenching mechanism for PA is induced by the energy transfer.

Furthermore, to confirm the FRET is happening in the detection of PA, time-resolved fluorescence spectroscopy was used to measure the fluorescence lifetime of the sensor in the absence and presence of varying concentrations of PA in THF/H_2O (1:9 v/v) mixture. As shown in Fig. 5b, the HPG-TPE presents a lifetime of 0.52 ns in the absence of

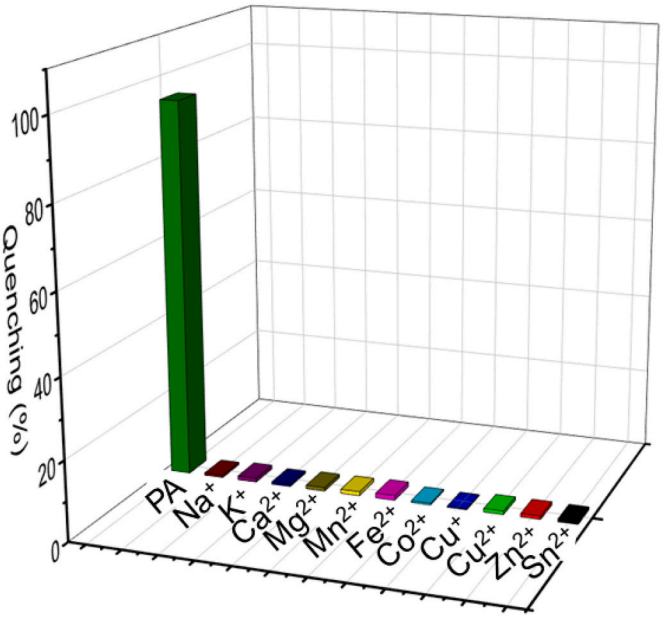

Fig. 6. Fluorescence quenching of HPG-TPE nanoparticles (10 μM) due to the addition of various metal ions and PA (90 μM).

PA. By the addition of different concentrations of PA to the HPG-TPE, the lifetime values of polymer remain unchanged. This result indicates that the quenching mechanism is static in nature and a ground state complex is formed between HPG-TPE and PA.

For the practical application of AIE-active HPG-TPE nanoparticles in environmental samples, various metal ions present in wastewater must be considered. Therefore, the sensitivity of the HPG-TPE nanoparticles was further analyzed in the presence of metal ions, such as Na^+, K^+, Ca^{2+}, Mg^{2+}, Mn^{2+}, Fe^{2+}, Co^{2+}, Cu^+, Cu^{2+}, Zn^{2+}, and Sn^{2+}. Fig. 6 shows that none of the metal ions tested had a fluorescence quenching effect on the HPG-TPE nanoparticles. In contrast, a drastic emission quenching occurs at the concentration of 90 μM of PA, suggesting that the addition of metal ions to the nanoparticles does not interfere with their efficiency at sensing PA.

From a practical perspective, it is extremely useful to develop portable sensors or smart devices for real-time and on-site detection. Assays performed on paper require small sample volumes, and paper sensors can be easily fabricated by immobilizing fluorescent materials on pieces of paper and tracing explosives can be visualized by an on/off fluorescence response under a UV lamp. To fabricate the paper sensor, a

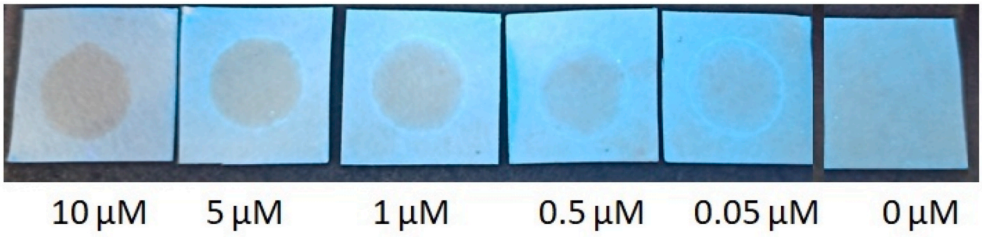

Fig. 7. Paper sensors fabricated by simply immersing filter paper in the HPG-TPE solution (10 μg mL^{-1} in THF), and fluorescence quenching in response to different concentrations of PA under UV irradiation.

small piece of filter paper was immersed in the solution of the HPG-TPE polymer in THF (10 μg mL^{-1}), followed by drying in air. The resulting paper sensor emitted a bright blue fluorescence under UV light, as shown in Fig. 7. A few drops of solution containing different PA concentrations from 0 to 10 μM were developed onto the paper sensor. The emission was progressively quenched, as expected, demonstrating the potential practical application of the HPG-TPE paper sensor for nitroaromatic explosive detection. Furthermore, HPG-TPE is soluble in common solvents, and HPG-TPE nanoparticles can easily be dispersed in water, making the fabrication of paper sensors effortless.

4. Conclusions

An AIE-active hyperbranched polymer was successfully synthesized by the polycondensation of HPG with diboronic acid-mediated TPE units via dynamic boronate ester linkages. The resultant HPG-TPE polymers formed nanoparticles with an average diameter of approximately 100 nm by the aggregation of TPE moieties in the THF/H_2O mixture (1:9 v/v). The HPG-TPE nanoparticles were tested for the detection of nitroaromatic explosives such as PA, DNP, NP, NT, and NM in aqueous solution. The nanoparticles exhibited fluorescence quenching in the order PA ≫ DNP > NP > NT > NM. The nanoparticles exhibited a high quenching efficiency specifically for PA with a quenching constant of 2.27×10^4 M^{-1}, which was calculated by fitting a linear plot to the Stern–Volmer equation. The limit of detection limit was 40 ppb. In addition, the highly soluble nature of HPG-TPE in organic solvents facilitates the fabrication of paper sensors that are practically applicable for PA detection.

CRediT authorship contribution statement

Nagendra Kalva: Investigation, Formal analysis, Writing – original draft. **Chinh Hoang Tran:** Project administration, Formal analysis, Writing – review & editing. **Min Woong Lee:** and, Funding acquisition, Data acquision, Formal analysis. **Rimesh Augustine:** Data acquision, Funding acquisition, Formal analysis. **Soo Jeong Lee:** Conceptualization, Writing – review & editing, Supervision, Funding acquisition.

Declaration of competing interest

The authors declare that they have no known competing financial interests or personal relationships that could have appeared to influence the work reported in this paper.

Acknowledgments

This work was supported by a National Research Foundation of Korea (NRF) grant funded by the Korean government (MSIT) (2021R1A2C2003685) and was partly supported by the Korea Institute of Energy Technology Evaluation and Planning (KETEP) grant funded by the Korean government (MOTIE) (20208401010080).

Appendix A. Supplementary data

Supplementary data to this article can be found online at https://doi.org/10.1016/j.dyepig.2021.109617

References

[1] Chen PC, Sukcharoenchoke S, Ryu K, Gomez de Arco L, Badmaev A, Wang C, Zhou C. 2,4,6-Trinitrotoluene (TNT) chemical sensing based on aligned single-walled carbon nanotubes and ZnO nanowires. Adv Mater 2010;22:1900–4.
[2] Lichtenstein A, Havivi E, Shacham R, Hahamy E, Leibovich R, Pevzner A, Krivitsky V, Davivi G, Presman I, Elnathan R, Engel Y, Flaxer E, Patolsky F. Supersensitive fingerprinting of explosives by chemically modified nanosensors arrays. Nat Commun 2014;5:4195.
[3] Yang Z, Dou X, Zhang S, Guo L, Zu B, Wu Z, Zeng H. A high-performance nitro-explosives Schottky sensor boosted by interface modulation. Adv Funct Mater 2015;25:4039–48.
[4] Guo L, Yang Z, Dou X. Artificial olfactory system for trace identification of explosive vapors realized by optoelectronic Schottky Sensing. Adv Mater 2017;29:1604528.
[5] Bastatas LD, Echeverria-Mora E, Wagle P, Mainali P, Austin A, McIlroy DN. Emergent electrical properties of ensembles of 1D nanostructures and their impact on room temperature electrical sensing of ammonium nitrate vapor. ACS Sens 2018;3:2367–74.
[6] Liu R, Li Z, Huang Z, Li K, Lv Y. Biosensors for explosives: state of art and future trends. Trends Anal Chem 2019;118:123–37.
[7] Li Y, Zhou W, Zu B, Dou X. Qualitative detection toward military and improvised explosive vapors by a facile TiO_2 nanosheet-based chemiresistive sensor array. Front. Chem 2020;8:1–12.
[8] Hebert RM, Jackovitz AM. In: Williams MA, Reddy G, Quinn MJ, editors. In wildlife toxicity assessments for chemicals of military concern. Johnson MS: Elsevier; 2015. p. 271–7. https://doi.org/10.1016/B978-0-12-800020-5.00015-6.
[9] Panigrahi A, Sahu BP, Mandani S, Nayak D, Giri S, Sarma TK. AIE active fluorescent organic nanoaggregates for selective detection of phenolic-nitroaromatic explosives and cell imaging. J Photochem Photobiol, A 2019;374:194–205.
[10] Wyman JF, Serve MP, Hobson DW, Lee LH, Uddin DE. Acute toxicity, distribution, and metabolism of 2,4,6-trinitrophenol (picric acid) in Fischer 344 rats. J Toxicol Environ Health 1992;37:313–27.
[11] Zhou H, Chua MH, Tang BZ, Xu J. Aggregation-induced emission (AIE)-active polymers for explosive detection. Polym Chem 2019;10:3822–40.
[12] Kovacic P, Somanathan R. Nitroaromatic compounds: environmentaltoxicity, carcinogenicity, mutagenicity, therapy and mechanism. J Appl Toxicol 2014;34:810–24.
[13] Nagarkar SS, Joarder B, Chaudhari AK, Mukherjee S, Ghosh SK. Highly selective detection of nitro explosives by a luminescentmetal–organic framework. Angew Chem Int Ed Engl 2013;52:2881–5.
[14] He G, Peng H, Liu T, Yang M, Zhang Y, Fang Y. A novel picric acid film sensor via combination of the surface enrichment effect of chitosan films and the aggregation-induced emission effect of siloles. J Mater Chem 2009;19:7347–53.
[15] Elsner M, Jochmann MA, Hofstetter TB, Hunkeler D, Bernstein A, Schmidt TC, Schimmelmann A. Current challenges in compound-specific stable isotope analysis of environmental organic contaminants. Anal Bioanal Chem 2012;403:2471–91.
[16] Walsh ME. Determination of nitroaromatic, nitramine, and nitrate ester explosives in soil by gas chromatography and an electron capture detector. Talanta 2001;54:427–38.
[17] Hallowell SF. Screening people for illicit substances: a survey of current portal technology. Talanta 2001;54:447–58.
[18] Jamil AKM, Sivanesan A, Izake EL, Ayoko GA, Fredericks PM. Molecular recognition of 2, 4, 6-trinitrotoluene by 6-aminohexanethiol and surface-enhanced Raman scattering sensor. Sens Actuators, B 2015;221:273–80.
[19] Popov IA, Chen H, Kharybin ON, Nikolaev EN, Cooks RG. Detection of explosives on solid surfaces by thermal desorption and ambient ion/molecule reactions. Chem Commun 2005:1953–5.
[20] Babaee S, Beiraghi A. Micellar extraction and high performance liquid chromatography-ultra violet determination of some explosives in water samples. Anal Chim Acta 2010;662:9–13.

[21] Najarro M, Dávila Morris ME, Staymates ME, Fletcher R, Gillen G. Optimized thermal desorption for improved sensitivity in trace explosives detection by ion mobility spectrometry. Analyst 2012;137:2614–22.
[22] Naddo T, Che Y, Zhang W, Balakrishnan K, Yang X, Yen M, Zhao J, Moore JS, Zang L. Detection of explosives with a fluorescent nanofibril film. J Am Chem Soc 2007;129:6978–9.
[23] Zhou L, Zhang H, Luan Y, Cheng S, Fan L-J. Amplified detection of iron ion based on plasmon enhanced fluorescence and subsequently fluorescence quenching. Nano-Micro Lett 2014;6:327–34.
[24] Sun X, Wang Y, Lei Y. Fluorescence based explosive detection: from mechanisms to sensory materials. Chem Soc Rev 2015;44:8019–61.
[25] Zhang Y, Li B, Ma H, Zhang L, Zhang W. An RGH–MOF as a naked eye colorimetric fluorescent sensor for picric acid recognition. J Mater Chem C 2017;5:4661–9.
[26] Huang X-L, Liu L, Gao M-L, Han Z-B. A luminescent metal–organic framework for highly selective sensing of nitrobenzene and aniline. RSC Adv 2016;6:87945–9.
[27] Satapathi S, Kokil A, Venkatraman BH, Venkataraman LLiD, Kumar J. Sensitive detection of nitroaromatics with colloidal conjugated polymer nanoparticles. IEEE Sensor J 2013;13:2329–33.
[28] Xu S, Lu H. Fluorescence based explosive detection: from mechanisms to sensory materials Biosens. Bioelectron 2016;85:950–6.
[29] Freeman R, Finder T, Bahshi L, Gill R, Willner I. Functionalized CdSe/ZnS QDs for the detection of nitroaromatic or RDX explosives. Adv Mater 2012;24:6416–21.
[30] Rochat S, Swager TM. Conjugated amplifying polymers for optical sensing applications. ACS Appl Mater Interfaces 2013;5:4488–502.
[31] Tanwar AS, Hussain S, Malik AH, Afroz MA, Iyer PK. Inner filter effect based selective detection of nitroexplosive-picric acid in aqueous solution and solid support using conjugated polymer. ACS Sens 2016;1:1070–7.
[32] Zhou H, Wang X, Lin TT, Song J, Tang BZ, Xu J. Poly(triphenyl ethene) and poly (tetraphenyl ethene): synthesis, aggregation-induced emission property and application as paper sensors for effective nitro-compounds detection. Polym Chem 2016;7:6309–17.
[33] Senthamizhan A, Celebioglu A, Bayir S, Gorur M, Doganci E, Yilmaz F, Uyar T. Highly fluorescent pyrene-functional polystyrene copolymer nanofibers for enhanced sensing performance of TNT. ACS Appl Mater Interfaces 2015;7: 21038–46.
[34] Nagarjuna G, Kumar A, Kokil A, Jadhav KG, Yurt S, Kumar J, Venkataraman D. Enhancing sensing of nitroaromatic vapours by thiophene-based polymer films. J Mater Chem 2011;21:16597–602.
[35] Zhao D, Swager TM. Sensory responses in solution vs solid state: a fluorescence quenching study of poly(iptycenebutadiynylene)s. Macromolecules 2005;38: 9377–84.
[36] Huang Y, Xing J, Gong Q, Chen L-C, Liu G, Yao C, Wang Z, Zhang H-L, Chen Z, Zhang Q. Reducing aggregation caused quenching effect through co-assembly of PAH chromophores and molecular barriers. Nat Commun 2019;10:169.
[37] Luo J, Xie Z, Lam JWY, Cheng L, Chen H, Qiu C, Kwok HS, Zhan X, Liu Y, Zhu D, Tang BZ. Aggregation-induced emission of 1-methyl-1,2,3,4,5-pentaphenylsilole. Chem Commun 2001:1740–1.
[38] Tang BZ, Zhan X, Yu G, Sze Lee PP, Liu Y, Zhu D. Efficient blue emission from siloles. J Mater Chem 2001;11:2974–8.
[39] Toal SJ, Jones KA, Magde D, Trogler WC. Luminescent silole nanoparticles as chemoselective sensors for Cr(VI). J Am Chem Soc 2005;127:11661–5.
[40] Hong Y, Häußler M, Lam JWY, Li Z, Sin KK, Dong Y, Tong H, Liu J, Qin A, Renneberg R, Tang BZ. Label-free fluorescent probing of G-quadruplex formation and real-timemonitoring of DNA folding by a quaternized tetraphenylethene salt withaggregation-induced emission characteristics. Chem Eur J 2008;14:6428–37.
[41] Hong Y, Xiong H, Lam JWY, Häußler M, Liu J, Yu Y, Zhong Y, Sung HHY, Williams ID, Wong KS, Tang BZ. Fluorescent bioprobes: structural matching in the docking processes of aggregation-induced emission fluorogens on DNA surfaces. Chem Eur J 2010;16:1232–45.
[42] Andrew TL, Swager TM. A fluorescence turn-on mechanism to detect high explosives RDX and PETN. J Am Chem Soc 2007;129:7254–5.
[43] Kim S, Pudavar HE, Bonoiu A, Prasad PN. Aggregation-enhanced fluorescence in organically modified silica nanoparticles: a novel approach toward high-signal-output nanoprobes for two-photon fluorescence bioimaging. Adv Mater 2007;19: 3791–5.
[44] Mahtab F, Yu Y, Lam JWY, Liu J, Zhang B, Lu P, Zhang X, Tang BZ. Fabrication of silica nanoparticles with both efficient fluorescence and strong magnetization, and exploration of their biological applications. Adv Funct Mater 2011;21:1733–40.
[45] Zhang X, Zhang X, Yang B, Hui J, Liu M, Chi Z, Liu S, Xu J, Wei Y. Novel biocompatible cross-linked fluorescent polymeric nanoparticles based on an AIE monomer. J Mater Chem C 2014;2:816–20.
[46] Kalva N, Uthaman S, Jang EH, Augustine R, Jeon SH, Huh KM, Park I-K, Kim I. Aggregation-induced emission-active hyperbranched polymer-based nanoparticles and their biological imaging applications. Dyes Pigments 2021;186:108975.
[47] Zhou H, Li J, Chua MH, Yan H, Tang BZ, Xu J. Poly(acrylate) with a tetraphenylethene pendant with aggregation-induced emission (AIE) characteristics: highly stable AIE-active polymer nanoparticles for effective detection of nitro compounds. Polym Chem 2014;5:5628–37.
[48] Liu J, Zhong Y, Lu P, Hong Y, Lam JWY, Faisal M, Yu Y, Wong KS, Tang BZ. A superamplification effect in the detection of explosives by a fluorescent hyperbranched poly(silylenephenylene) with aggregation-enhanced emission characteristics. Polym Chem 2010;1:426–9.
[49] Qin A, Lam JWY, Tang L, Jim CKW, Zhao H, Sun J, Tang BZ. Polytriazoles with aggregation-induced emission characteristics: synthesis by click polymerization and application as explosive chemosensors. Macromolecules 2009;42:1421–4.
[50] Wang X, Guo Y, Li D, Chen H, Sun R-C. Fluorescent amphiphilic cellulose nanoaggregates for sensing trace explosives in aqueous solution. Chem Commun 2012:5569–71.
[51] Wang C, Wang QLiB, Li D, Yu J. Fluorescent sensors based on AIEgen-functionalised mesoporous silica nanoparticles for the detection of explosives and antibiotics. Inorg Chem Front 2018;5:2183–8.
[52] Zhou S, Gu P, Wan H, Zhu Y, Wang A, Shi H, Xu Q, Lu J. TPE-containing amphiphilic block copolymers: synthesis and application in the detection of nitroaromatic pollutants. Polym Chem 2020;11:7244–52.
[53] Nawaz MAH, Meng L, Zhou H, Ren J, Shahzad SA, Hayat A, Yu C. Tetraphenylethene probe based fluorescent silica nanoparticles for the selective detection of nitroaromatic explosives. Anal Methods 2021;13:825–31.
[54] Dong W, Fei T, Scherf U. Conjugated polymers containing tetraphenylethylene in the backbones and side-chains for highly sensitive TNT detection. RSC Adv 2018;8: 5760–7.
[55] Nabeel F, Rasheed T, Mahmood MF, Khan SU-D. Hyperbranched copolymer based photoluminescent vesicular probe conjugated with tetraphenylethene: synthesis, aggregation-induced emission and explosive detection. J Mol Liq 2020;308: 113034.
[56] Li H, Wu H, Zhao E, Li J, Sun JZ, Qin A, Tang BZ. Hyperbranched poly (aroxycarbonyltriazole)s: metal-free click polymerization, light refraction, aggregation-induced emission, explosive detection, and fluorescent patterning. Macromolecules 2013;46:3907–14.
[57] Abbina S, Vappala S, Kumar P, Siren EMJ, La CC, Abbasi U, Brooks DE, Kizhakkedathu JN. Hyperbranched polyglycerols: recent advances in synthesis, biocompatibility and biomedical applications. J Mater Chem B 2017;5:9249–77.
[58] Wilms D, Stiriba S-E, Frey H. Hyperbranched polyglycerols: from the controlled synthesis of biocompatible polyether polyols to multipurpose applications. Acc Chem Res 2010;43:129–41.
[59] Sunder A, Mülhaupt R, Haag R, Frey H. Hyperbranched polyether polyols: a modular approach to complex polymerarchitectures. Adv Mater 2000;12:235–9.
[60] Huang H, Liu M, Chen J, Mao L, Wan Q, Wen Y, Deng F, Zhou N, Zhang X, Wei Y. Fabrication of β-cyclodextrin containing AIE-activepolymeric composites through formation of dynamicphenylboronic borate and their theranostic applications. Cellulose 2019;26:8829–41.
[61] Tran CH, Lee MW, Kim SA, Jang HB, Kim I. Kinetic and Mechanistic Study of Heterogeneous double metal cyanide-catalyzed ring-opening multibranching polymerization of glycidol. Macromolecules 2020;53:2051–60.
[62] Khabarov YG, Patrakeev AA, Veshnyakov VA, Kosyakov DS, Ul'yanovskii NV, Garkotin AY. One-step synthesis of picric acid from phenol. Org Prep Proced Int 2017;49:178–81.
[63] Xiong J-F, Li J-X, Mo G-Z, Huo J-P, Liu J-Y, Chen X-Y, Wang Z-Y. Benzimidazole derivatives: selective fluorescent chemosensors for the picogram detection of picric acid. J Org Chem 2014;79:11619–30.
[64] Bhalla V, Gupta A, Kumar M. Fluorescent nanoaggregates of pentacenequinone derivative for selective sensing of picric acid in aqueous media. Org Lett 2012;14: 3112–5.
[65] Wu Y, Chen Q, Li Q, Lu H, Wu X, Ma J, Gao H. Daylight-stimulated antibacterial activity for sustainable bacterial detection and inhibition. J Mater Chem B 2016;4: 6350–7.
[66] Nayak JN, Aralaguppi MI, Naidu BVK, Aminabhavi TM. Thermodynamic properties of water + tetrahydrofuran and water + 1,4-dioxane mixtures at (303.15, 313.15, and 323.15) K. J Chem Eng Data 2004;49:468–74.